Quaternary Science Reviews 227 (2020) 106051

Contents lists available at ScienceDirect

Quaternary Science Reviews

journal homepage: www.elsevier.com/locate/quascirev

A Holocene history of the Indian monsoon from Qilu Lake, southwestern China

Aubrey L. Hillman [a, *], Ryan F. O'Quinn [a], Mark B. Abbott [b], Daniel J. Bain [b]

[a] Department of Environmental Science, School of Geosciences, University of Louisiana at Lafayette, 611 McKinley St, Lafayette, LA 70504, USA
[b] Department of Geology and Environmental Science, University of Pittsburgh, 4107 O'Hara St, Pittsburgh, PA 15260, USA

ARTICLE INFO

Article history:
Received 14 June 2019
Received in revised form
31 October 2019
Accepted 6 November 2019
Available online 19 November 2019

Keywords:
Holocene
Paleoclimatology
Stable isotopes
Indian Summer Monsoon
China

ABSTRACT

Understanding the magnitude, nature, and forcing mechanisms of past abrupt changes in Indian Summer Monsoon (ISM) strength is central to characterizing future manifestations in the face of global climate change, particularly at centennial time scales. Here we summarize a 6200 year record of oxygen isotopes from Lake Qilu in Yunnan Province, China. The lake is sensitive to changes in precipitation-evaporation balance and precipitates calcite, potentially providing insight into past hydroclimate through oxygen isotope analysis. Beginning at 5200 cal years BP, oxygen isotopes shift to higher values, indicative of a period of aridity and lower lake levels which persist until 3600 cal years BP. Thereafter, lake levels are extraordinarily stable until 1500 cal years BP. At 1500 cal years BP, measurable anthropogenic impacts occur, resulting in the delivery of red, iron-rich catchment soil to the lake and higher oxygen isotope values. These changes are likely the result of land clearance for the expansion of agricultural activities. The Qilu record is remarkably consistent with the record from Xingyun Lake, 10 km to the north, strongly suggesting that regional climate drivers are responsible for the changes after 5200 cal years BP and then the stability from 3600 to 1500 cal years BP. Comparison of both these records with Dongge Cave illustrate the importance of evaporative enrichment in driving higher oxygen isotope values from 5200 to 3600 cal years BP.

1. Introduction

The Indian Summer Monsoon (ISM) is a vital source of water for large portions of Asia. A timely arrival of the monsoon with sufficient strength can result in adequate water for agriculture, aquaculture, and hydroelectric power generation, but late or early arrivals coupled with weak or strong conditions can result in either drought or flooding conditions. Therefore, understanding the ISM's variability has important implications for water resources, safety, and livelihood. Freshwater lakes are one such water resource and can act as a storage system for ISM precipitation and provide reserves in drought years. Hence clarification of the history of human interactions with freshwater resources reveals how these interactions may evolve in the future. This is particularly relevant in the face of present-day climate change, as human exploitation of water resources are generally poorly resilient to shifts in ISM strength trends. Examining paleoclimate records to understand the magnitude of ISM variability that can be expected on decadal and centennial timescales can inform our understanding of the management of freshwater resources.

In regions of SE Asia most affected by the ISM, a set of diverse paleoclimate records have been published that suggest measurably dry conditions in the middle Holocene, broadly from 5 to 4 ka (Berkelhammer et al., 2012; Bird et al., 2014; Cai et al., 2012; Fleitmann et al., 2007; Gebregiorgis et al., 2016; Govil and Naidu, 2011; Hong et al., 2014, 2018; Kathayat et al., 2018; Rashid et al., 2011; Sarkar et al., 2015). However the spatial extent, severity, rapidity, and cause of this event is unclear, necessitating a greater number of records from a variety of archives that record precipitation and evaporation changes. Our understanding of this shift in the ISM is additionally complicated by the East Asian Summer Monsoon (EASM), a separate and distinct system from the ISM, which is more important for regions of eastern China, and whose records do not always manifest this abrupt change during 5-4 ka. Because the boundaries between the ISM and EASM shift from year to year, regions that lie in the transition zone may provide valuable information regarding the nature of ISM and EASM synchronicity and interactions.

* Corresponding author.
E-mail address: aubrey.hillman@louisiana.edu (A.L. Hillman).

https://doi.org/10.1016/j.quascirev.2019.106051
0277-3791/

We present here a sediment core record from Qilu Lake, a lake approximately 70 km south of Kunming, the capital of the Yunnan Province, and a region of China that lies within the transition zone of the ISM and EASM. We primarily use oxygen ($\delta^{18}O$) and carbon ($\delta^{13}C$) isotopes of authigenically precipitated calcite to infer changes in lake level driven by shifts in precipitation and evaporation. The objective of this study is to consider the combined effects of climate and anthropogenic forcings on abrupt shifts in lake level. In doing so, the aims of this study are to 1) to characterize centennial- and millennial-scale Holocene trends in hydroclimate and integrate these results with previous studies and 2) to characterize the timing and nature of human interactions with water resources over the last few millennia to understand anthropogenic controls on lake hydrologic balance.

2. Background

2.1. Monsoonal climate

The Yunnan Province has a subtropical highland climate with short, cool, dry winters, and long, warm and humid summers (Kottek et al., 2006). Average annual precipitation totals 1001 mm and has a highly seasonal distribution with 75–80% falling between the months of June and September. The prevailing wind direction in the summer months means that Yunnan is predominantly affected by the ISM, however this region lies within the transition zone of the ISM and EASM domains (Zhang, 1988). HYSPLIT back-trajectory analysis data from the last 15 years confirms that the prevailing wind from June–August is from the west and southwest and thus more influenced by the ISM in most years (Hillman et al., 2017); however, it is unknown how this pattern may have changed over longer timescales and indeed throughout the Holocene.

The Global Network of Isotopes in Precipitation (GNIP) has a station in Kunming that has monthly precipitation isotope data that span 1986-2003 AD. As has been previously established, there is a moderately good negative correlation ($R^2 = 0.37$, $p < 0.01$) between precipitation $\delta^{18}O$ values and monthly precipitation amount and a moderately weak negative correlation ($R^2 = 0.19$, $p = 0.02$) between precipitation $\delta^{18}O$ values and monthly temperature at this station (Hillman et al., 2017). Previous research has concluded that the predominant control on $\delta^{18}O$ values within precipitation in the Kunming region is precipitation amount arriving during summer monsoon season and that there is minimal influence from the seasonal change in atmospheric temperature (Araguás-Araguás et al., 1998), which is confirmed by the GNIP data. This likely arises from several upstream air mass processes such as rainout, distillation, and vertical convective activity, all leading to lower $\delta^{18}O$ values during periods of intense precipitation (Vuille et al., 2005).

It has been rigorously established by speleothem records over multi-millennial timescales (as summarized in Cheng et al., 2012) that the strength of the ISM is well-correlated to changes in summer insolation, which is in turn mainly forced by the orbital parameter of precessional forcing (Kutzbach, 1981). On centennial and decadal time-scales, controls on ISM strength appear to be more spatially and temporally variable. Several speleothem records have found connections to abrupt decreases in ISM strength and Northern Hemisphere temperatures through occurrences such as Heinrich and Bond Events (Wang et al., 2001, 2005). These events are hypothesized to have caused a southerly shift in the intertropical convergence zone (ITCZ), resulting in a weaker ISM and less rainfall penetrating into mainland Asia.

Others have noted connections to Pacific sea surface temperatures (SSTs) driven by the El Niño Southern Oscillation (ENSO) and its influence on the temperature gradient of the Indian Ocean. During El Niño events, anomalously warm SSTs in the eastern Pacific shift the Walker circulation cell eastward and reduce atmospheric convergence in the eastern Indian Ocean (Berry and Reeder, 2014). This increases Indian Ocean SSTs, which reduces the land-ocean thermal contrast, and delays the onset of monsoon conditions leading to lower annual precipitation (Prodhomme et al., 2014). Another important factor is the Indian Ocean Dipole (IOD), which is the E-W gradient in SSTs across the Indian Ocean (Saji et al., 1999). However, the IOD can itself be influenced by the strength of the ISM which generates winds that influence upwelling (Abram et al., 2007) and the IOD has potentially complex interactions with ENSO activity, which may have changed throughout the Holocene (Abram et al., 2008). It is difficult to make generalizations because of this substantial variability in the IOD, but previous work using corals suggests that in the middle Holocene IOD events frequently occurred and interacted with El Niño events which may have led to prolonged dry periods (Abram et al., 2007).

2.2. Lake setting

Qilu (24°10′N, 102°45′E, 1797 m elevation, Fig. 1C) is a fairly large (36 km^2) and shallow lake compared to others in the region. It has a maximum depth of ~7 m and an average depth of 4 m (Whitmore et al., 1997) although lake levels can vary up to several meters on a seasonal to annual basis (Brenner et al., 1991). The lake basin formed from a combination of tectonic faulting and dissolution of carbonate bedrock (Wang et al., 1998). Anthropogenic land-building along the southern and western shores of the lake has been extensive, as evidenced by unnaturally straight shorelines that appear on satellite imagery, but it is unknown when this land-building took place. Qilu's catchment area is ~200 km^2 and the surficial geology is dominated by Quaternary alluvium, dolomite, limestone, and small portions of metamorphic rocks (Fig. 1B). The lake receives inflowing water from 10 intermittent streams and multiple small springs. Qilu loses water to karst systems in a channel in Tonghai County, but this is controlled to facilitate irrigation. The magnitude of this water loss remains unquantified but is likely negligible to the water budget as lake water isotopic composition samples demonstrate that the lake behaves as a closed-basin.

Using the GNIP station data, we calculated that the average weighted $\delta^{18}O$ composition of precipitation falling in the Kunming region should be −9.9‰ VSMOW (Fig. 2). A water sample collected from Qilu in May 2019 had a $\delta^{18}O$ values of −4.25‰ VSMOW and a sample collected in 1994 AD measured −5.9‰ VSMOW (Whitmore et al., 1997). Both samples demonstrate that Qilu water has higher $\delta^{18}O$ values compared to average annual precipitation. This suggests that Qilu behaves as a closed-basin lake that loses the majority of its water through evaporative processes. Therefore, while Qilu may be a surficially open lake that loses some amount of water to groundwater throughflow, the strongest influence on lake hydrologic balance is evaporation.

Qilu has experienced significant water quality issues in recent years. It has a trophic status index that classifies it as eutrophic with high concentrations of nitrogen and Secchi depth <1 m (Liu et al., 2012). The lake receives untreated wastewater from fertilizer and textile plants as well as domestic sewage and farmland runoff (Whitmore et al., 1997). High concentrations of Pb, Cu, and Zn have also been noted in the surface sediments, likely from industrial activities (Liu et al., 2007).

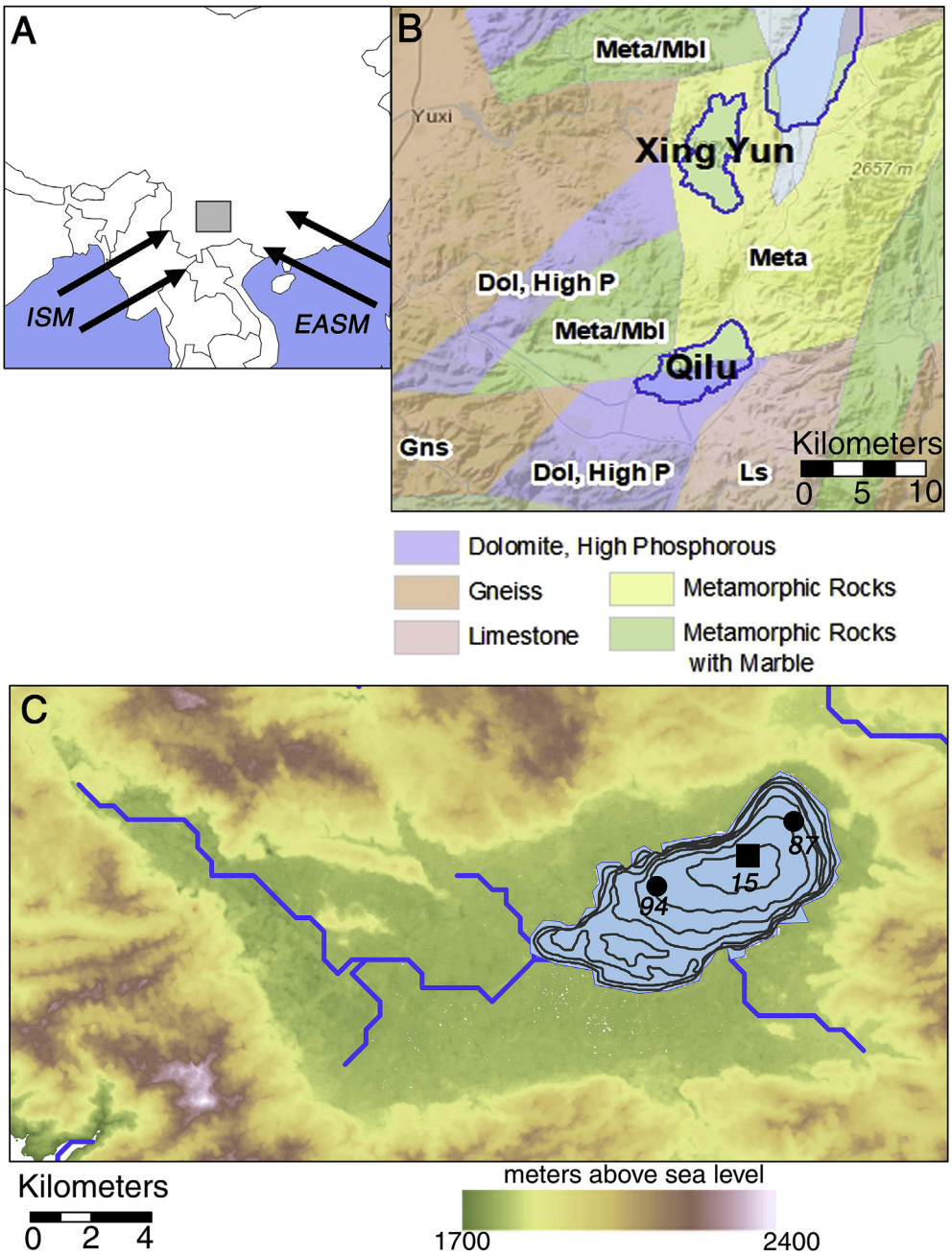

Fig. 1. A- Qilu Lake (gray square) with generalized direction of ISM and EASM winds; B) Qilu and nearby Xingyun Lake and surficial geology (Yunnan Province Bureau of Geology and Mineral Resources, 1990); C) Digital Elevation Model (DEM) of Qilu catchment. Coring locations of Brenner et al. (1991) (87) and Hodell et al (1999) (94) are marked by black circles. The coring location of this study (15) is marked by the black square. Lake bathymetry is in 1 m contour intervals (Hodell et al., 1999).

2.3. Previous lake sediment studies

Sediment cores were initially collected from Qilu in 1987 AD near the depocenter (Fig. 1C) and to a depth of 11 m (Brenner et al., 1991). Age control was provided by seven bulk sediment radiocarbon dates which had several reversals. Initial work focused on sediment geochemical composition and included analysis of weight percent carbon and nitrogen as well as trace elements such as Pb and Zn. Given the large chronological uncertainty, firm conclusions regarding geochemical variations down-core were difficult to make, but suggested a wet period at the beginning of the Holocene. The uppermost 80 cm of sediments were noted to be clay-rich, organic and carbonate poor, with high concentrations of Pb, Zn, Fe, and Al. This unit was interpreted to be the result of land clearance and sediment inwash associated with recent (post-industrial) human settlement.

Subsequent study of sediment cores from Qilu focused on 13.5 m of core collected in 1994 from the western side of the lake in a slightly shallower depth (Fig. 1C) (Hodell et al., 1999). Age control was provided by fourteen radiocarbon dates which were a combination of bulk sediment, shells, and a few terrestrial macrofossils. All but six of these dates were rejected due to stratigraphic reversals and the basal age of the core was estimated to be 50,000 years on the basis of extrapolation of sedimentation rates. Analysis focused on percent carbon and nitrogen, grain size, magnetic susceptibility, and the $\delta^{18}O$ values of carbonate minerals. $\delta^{18}O$ varied

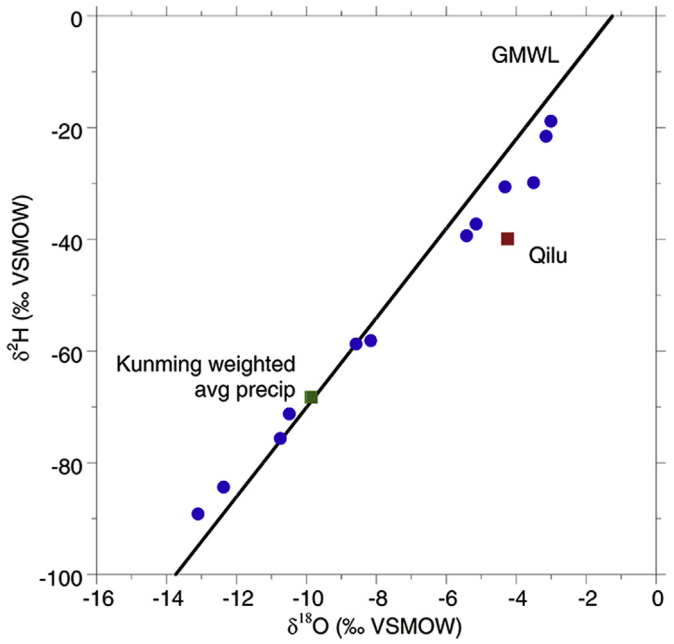

Fig. 2. IAEA/GNIP station data for Kunming values from 1986 to 2003. Precipitation $\delta^{18}O$ versus δD showing the global meteoric water line (GMWL) with monthly average values (blue circles). The green square is the average weighted composition of Kunming precipitation and the red square is Qilu lake water from 2019. (For interpretation of the references to color in this figure legend, the reader is referred to the Web version of this article.)

by nearly 6‰ and had several rapid and large magnitude shifts, particularly within the upper 2.0 m. One of the overarching conclusions of this study was that summer monsoon strength, as indicated by $\delta^{18}O$ values and supported by magnetic susceptibility values, responded to insolation forcing in the Northern Hemisphere over the late Pleistocene and Holocene. However re-examination of this record in conjunction with data from new cores at Xingyun Lake suggests there are a number of unconformities within the cores recovered in the 80s and 90s covering the pre-Holocene section of the record (Chen et al., 2014).

These two previous studies of Qilu sediment had several limitations, especially regarding chronology. Bulk sediment radiocarbon dates from lakes in karstic areas, as well as shell radiocarbon dates, may be subject to hard-water effects (Deevey et al., 1954). This may have contributed to the stratigraphic reversals that were noted in both studies. Additionally, the timing of events such as the accumulation of metals in the uppermost sediments or the age of the base of the 13.4 m core are highly uncertain due to extrapolation. Sedimentation rates have likely been highly variable over both these time periods, particularly with human activities, and possible hiatuses in sedimentation were noted by Brenner et al. (1991) as an additional complication. Additionally, the role that tectonics plays in influencing sedimentation rates is uncertain, but Qilu is surrounded on all sides by active faults, which have triggered earthquakes, particularly in the 1700's AD (Wen et al., 2008). Nonetheless, both previous studies provide valuable information about the nature of Qilu sediments and in particular, the Hodell et al (1999) study provides evidence that the $\delta^{18}O$ values of carbonate track summer monsoon strength.

The objective of this study is to build on previous work and to focus attention on producing a higher-resolution (every 2 cm) record of $\delta^{18}O$ values. The Hodell et al (1999) study had comparatively low resolution analysis (every 5–10 cm) of $\delta^{18}O$, which limits our understanding of the nature and timing of the abrupt changes that were observed in the upper 2.0 m. Additionally, $\delta^{18}O$ values were measured on bulk carbonate material which may include biogenic material, such as shells, that are subject to vital effects and not wholly reflective of variations in climate (Leng and Marshall, 2004). The data we present here is based on an independent age model created using Accelerator Mass Spectrometry (AMS) radiocarbon dates of charcoal and plant macrofossils and a high sampling resolution (one sample every 20–40 years) for $\delta^{18}O$ values on sieved, authigenic carbonate material.

3. Materials and methods

3.1. Core collection

Cores from Qilu were collected in August 2015 from the deepest part of the lake (Fig. 1C), which was 4.2 m depth at the time, using a steel barrel Livingston corer (Wright et al., 1984). Six 1-m long drives were collected in overlapping sections to produce a 3.90 m long composite record. Overlapping sections of core were correlated on the basis of visible stratigraphy (such as the transition to red clay at ~0.6 m) and sediment geochemistry (such as weight percent carbonate and $\delta^{18}O$ values). Additionally, a 0.65 m surface core that preserved the sediment-water interface was collected using a light weight percussion coring system. This surface core was extruded in the field at 0.5 cm intervals and used for ^{210}Pb dating and other analyses.

3.2. Age control

Radiocarbon ages were measured on seven samples of charcoal and plant macrofossils (Table 1). Samples were pretreated using a standard acid, base, acid procedure (Olsson, 1986) and processed and analyzed at the W.M. Keck Carbon Cycle Accelerator Mass Spectrometry Laboratory at the University of California, Irvine. The resulting ages were calibrated using CALIB 7.0 and the INTCAL13 calibration curve (Reimer et al., 2013). The upper 22 cm of the surface core sediments were lyophilized and analyzed for ^{210}Pb and ^{214}Pb activities by direct gamma (γ) counting in a broad energy germanium detector (Canberra BE-3825) at the University of Pittsburgh. Sediment ages for the surface were calculated using the Constant Rate of Supply (CRS) method, which accounts for variability in sediment flux, according to the methodology of Binford (1990). A composite age-depth model was developed using the ^{210}Pb ages and calibrated macrofossil radiocarbon dates. The resulting calibrated dates were used in the BACON code which uses Markov chain Monte Carlo statistics to create age-depth models and uses posterior probabilities to determine radiocarbon outliers (Blaauw and Christen, 2011) in the statistical software package "R" (R Core Development Team, 2008) (Fig. 3).

3.3. Geochemistry

Density and loss on ignition were measured at 2-cm intervals using 1 cm^3 samples. Samples were dried at 60 °C for 48 h to remove water and weighed for dry bulk density. Weight percent organic matter and carbonate content were determined by loss-on-ignition (LOI) at 550 °C and 1000 °C, respectively (Dean, 1974). Sediment magnetic susceptibility (MS) was measured on all split cores at room temperature using a Bartington® Instruments Ltd. ME2EI surface-scanning sensor equipped with a TAMISCAN-TSI automatic logging conveyer. Because surface samples were extruded into bags at 0.5 cm intervals, magnetic susceptibility for the uppermost sediments was not measured. Samples for powder X-ray diffraction (XRD) analysis were taken every 50 cm, lyophilized, and homogenized with an agate mortar and pestle. The

Table 1
AMS radiocarbon dates from Qilu cores.

UCI Number	Composite Core Depth (cm)	Material	^{14}C age (BP)	Error ±	Median Probability Calibrated Age (yr BP)	2σ Calibrated Age Range (yr BP)
180959	69.5	Charcoal	1205	15	1126	1069 to 1179
180960	107.5	Charcoal	1380	15	1298	1284 to 1310
201169	129.5	Charcoal	1795	15	1720	1630 to 1812
180961[a]	222.0	Leaf	3330	35	3564	3466 to 3677
201170	256.0	Charcoal	3105	15	3333	3253 to 3375
180962	299.0	Charcoal	4300	15	4855	4841 to 4866
164743	342.5	Charcoal	4505	45	5162	4980 to 5308

[a] Denotes date excluded from age model.

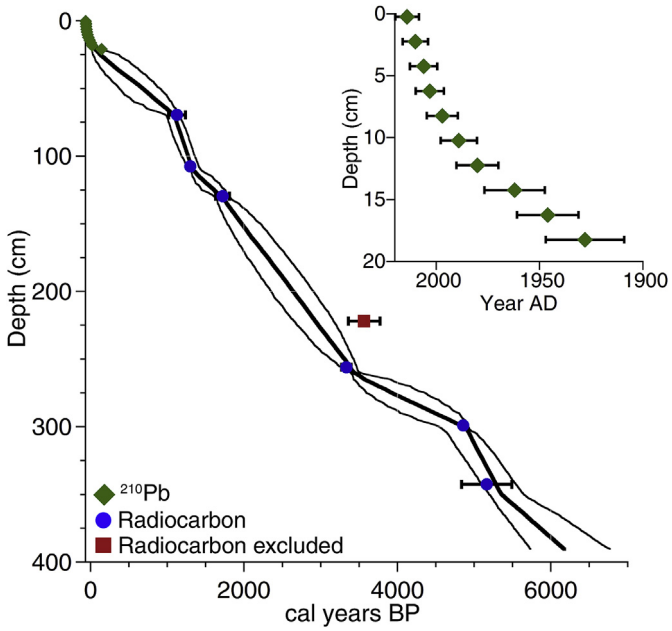

Fig. 3. Age-depth model with 95% confidence intervals. ^{210}Pb dates (green diamonds) and radiocarbon dates (blue circles) are plotted with 2 sigma error bars. Inset- ^{210}Pb dates. (For interpretation of the references to color in this figure legend, the reader is referred to the Web version of this article.)

samples were prepared as back-filled cavity mounts and analyzed using a DIANO 2100E X-ray Diffractometer at the University of Louisiana at Lafayette to identify the carbonate mineral phase. Samples were also analyzed on a Hitachi S3000N Scanning Electron Microscope (SEM) to examine crystal structure and morphology.

The composite core sequence was sampled at 2 cm intervals for $\delta^{18}O$ $\delta^{13}C$ values. Approximately 5 samples from each drive were analyzed through overlapping sections to check for consistency. Samples were disaggregated with 7% H_2O_2 and sieved through a 63-μm screen to remove biological carbonates derived from shells. The resulting fine-grained carbonate sediment was oxidized with a dilute (~3%) bleach solution, rinsed three times with Milli-Q water, frozen, lyophilized, and homogenized using an agate mortar and pestle. Bulk carbonate samples were reacted in ~100% phosphoric acid under vacuum at 70 °C. Samples were measured using an automated carbonate preparation device (KIEL-III) coupled to a gas-ratio mass spectrometer (Finnigan MAT 252) at the Environmental Isotope Laboratory, University of Arizona. Measurements were calibrated to the NBS-18 and NBS-19 calcite standards and values are reported in standard delta (δ) notation as the per mil (‰) deviation from Vienna Pee Dee Belemnite (VPDB). One sigma analytical uncertainties on the standards are within ±0.10‰ for $\delta^{18}O$ and ±0.08‰ for $\delta^{13}C$.

3.4. Lake bathymetry

Lake bathymetric data presented in Fig. 1C is based on data from Hodell et al (1999). ASTER global Digital Elevation Maps (DEMs) were used to create a map of 1 m contour intervals within the lake catchment. These 1 m intervals within the lake and in the surrounding catchment were used to calculate surface area and volume. Relationships of surface area, volume, and surface area to volume ratio were calculated relative to present day lake depth in order to explore how increases/decreases in lake level might change evaporation rates.

4. Results

The age-depth model indicates that the 3.90 m of core from Qilu spans the last ~6.2 ka (Fig. 3). While ideally additional radiocarbon ages would have been measured on samples from between 129.5 and 222 cm total composite depth and from below 342.5 cm down to the base of the core, there were simply no macrofossils of sufficient size to be dated. Bulk sediment radiocarbon dates are inappropriate in this situation because of the prevalence of limestone and dolomite within the lake catchment (Fig. 1C). The presence of carbonate material may result in the inclusion of aged material in bulk sediment dates, creating anomalously old ages (Deevey et al., 1954), which do not remain consistently offset from terrestrial dates when lake levels fluctuate (Geyh et al., 1997). Since one of the goals of this study was to avoid such chronological errors that may have been present in the previous work on Qilu by Brenner et al. (1991) and Hodell et al (1999), we have avoided the use of such material to create an age-depth model. While this yields greater uncertainty in the timing of events between ~3500 and 1800 cal years BP and prior to 5200 cal years BP, this overall yields more certainty to the age model where macrofossil radiocarbon ages do exist. There is one date from 222 cm composite depth, which is slightly older than would otherwise be expected. The material of this sample was a leaf whereas all the other dates were composed of charcoal. Charcoal is friable and unlikely to sit on the landscape for a long period of time before washed into the lake, thus it reflects as close to a "true" age of deposition as can be estimated in lake sediments. However, a leaf is more likely to sit on the surrounding lake catchment before being washed in, which may result in a radiocarbon age that is "older" (Abbott and Stafford, 1996). This sample was also small and approached the limits of size necessary to obtain an accurate radiocarbon age, making it more susceptible to error (Wohlfarth et al., 1998). Age uncertainty is highest at the base of the core, but above 3.42 m composite depth, uncertainty associated with the BACON age model is ±300 years, and frequently closer to ±200 years.

Sediment from 3.90 to 2.30 m (~6.2–3.0 ka) is homogenous green/gray silt and clay with no visible sedimentary structures and is comprised of between 10 and 50% carbonate material (Fig. 4). Beginning at a depth of 2.30 m (3.0 ka), sediment gradually

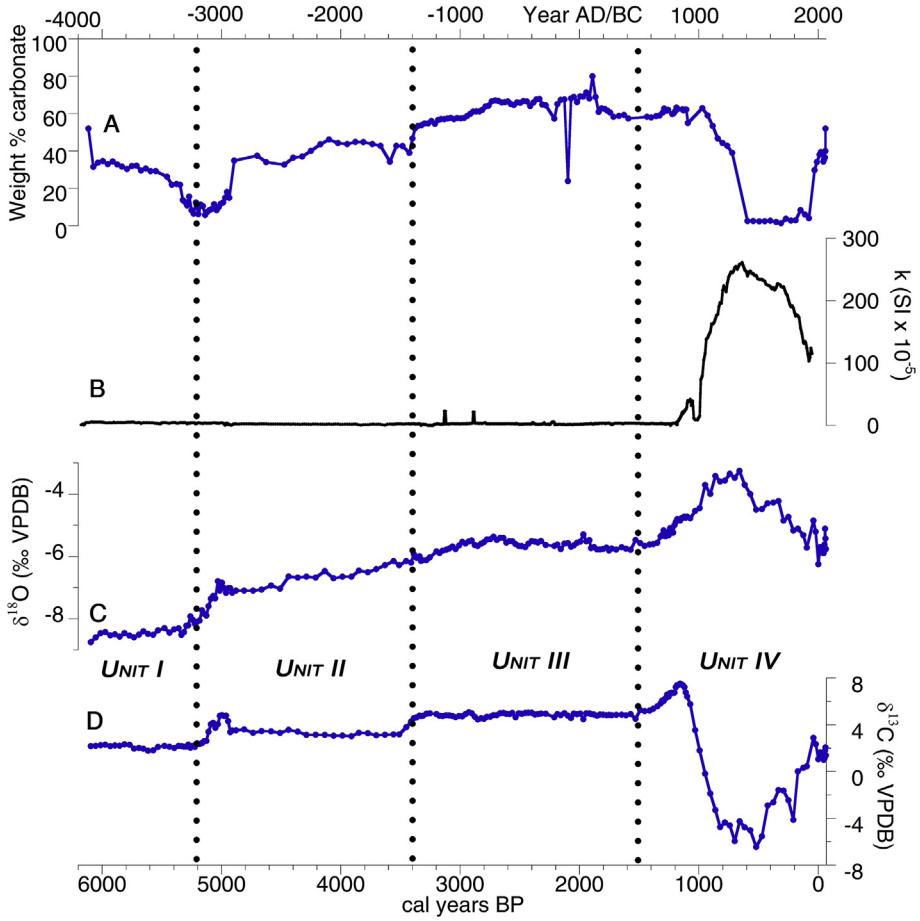

Fig. 4. A) Percent carbonate estimated by LOI 1000 °C; B) Magnetic susceptibility; C) Oxygen isotopes; D) Carbon isotopes divided into Units I-IV.

transitions to a homogenous lighter gray color with a higher carbonate content of ~70%. From 3.90 to 2.30 m, magnetic susceptibility values are very low (<10 SI units) and stable. In the upper 0.60 m (~0.9 ka), carbonate material abruptly declines and sediments are composed of red, iron-rich, very fine-grained clay sediments. This is accompanied by a rapid increase in magnetic susceptibility values to a peak of 260 SI units at 650 cal years BP before gradually declining back to values ~100 SI units. The most recent 100 years of sediment have increases in carbonate to 50%.

XRD analyses indicate that the primary carbonate mineral phase is calcite and SEM images indicate that it is euhedral to slightly subhedral in form (Fig. S1). $\delta^{18}O$ values range from −8.75‰ to −3.25‰ VPDB (Fig. 4). $\delta^{13}C$ values show more variable trends and range from −6.44‰ to +7.39‰ VPDB. In this manuscript we will primarily focus on $\delta^{18}O$ and use $\delta^{13}C$ to investigate covariance, which can be indicative of changes in hydrologic conditions, such as open versus closed status (Talbot, 1990) and to understand variations in CO_2 exchange with the atmosphere (Li and Ku, 1997). On the basis of major features and isotope data, we divide the record into four units. ***Unit I- 6.2 to 5.2 ka:*** **$\delta^{18}O$ values** are stable at −8.47 ± 0.11‰ and $\delta^{13}C$ values are stable at +2.13 ± 0.15‰. *Unit II- 5.2 to 3.6 ka:* $\delta^{18}O$ first abruptly increases from −8.43 to −6.79‰ by 5.0 ka and then more gradually increases to −6.28‰ by the end of the unit. $\delta^{13}C$ display an abrupt increase to +4.78‰ by 5.0 ka, then decline to a stable average of +3.31‰. *Unit III- 3.6 to 1.5 ka:* $\delta^{18}O$ shows a slight increase of ~0.60‰ followed by mostly stable values around −5.70‰. $\delta^{13}C$ initially increases by 1.20‰, then is extremely stable at an average of +4.87 ± 0.15‰. Covariance between $\delta^{18}O$ and $\delta^{13}C$ within Units I-III is high with an R^2 value of 0.85 ($p < 0.05$) (Fig. 5). *Unit IV- 1.5 ka to present:* $\delta^{18}O$ initially shows a pronounced and rapid trend to −3.35‰ by 0.75 ka before declining to −5.76‰ in the most recent sediments. $\delta^{13}C$ initially increases to +7.39‰ at 0.12 ka before substantially declining to −6.44‰ at 0.5 ka and then increasing to around +2‰. Covariance between $\delta^{18}O$ and $\delta^{13}C$ within Unit IV is lower with an R^2 value of 0.30 ($p < 0.05$).

5. Discussion

5.1. Modern isotope calibration

The $\delta^{18}O$ value of authigenic calcite can be used to reconstruct the $\delta^{18}O$ value of the lake water during the time of formation when accounting for a predictable temperature dependent water-calcite transformation (Equation (1)).

$$1000 ln\alpha(Calcite - H_2O) = 18.03\left(10^3 T^{-1}\right) - 32.42 \left(\text{Kim and O'Neil, 1997}\right) \quad (1)$$

Since lake water isotopes in closed-basins can provide insight into lake hydrologic shifts due to changes in the balance between precipitation and evaporation (P-E balance), down-core $\delta^{18}O$ analysis of carbonate minerals can therefore be used to understand variations in hydroclimate. Given Qilu behaves as a closed-basin lake (Fig. 2), we surmise that precipitating calcite will therefore

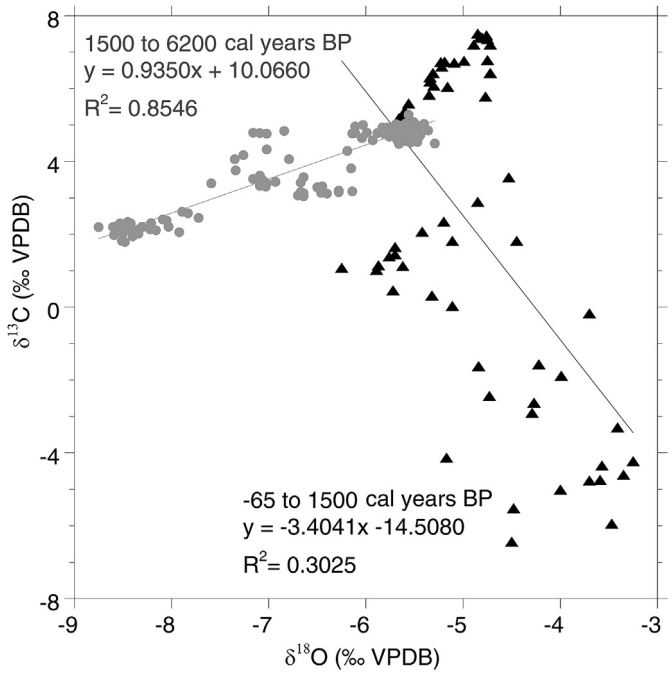

Fig. 5. Covariance of oxygen and carbon isotopes for 6200-1500 cal years BP in dark gray circles and for 1500 to −65 cal years BP in black triangles.

reflect variations in lake hydrology, driven by the combined changes in the strength of the ISM (precipitation) and aridity (evaporation) through the Holocene. One additional factor to consider in interpreting $\delta^{18}O$ values of calcite is the influence of temperature. Increasing temperature may result in increasing $\delta^{18}O$ values arising from a combination of vapor to liquid fractionation (+0.60‰/1 °C) (Rozanski et al., 1993) and an opposing water to calcite fractionation (−0.24‰/1 °C) (Craig, 1965). However, the sum magnitude of these changes (+0.36‰/1 °C) tends to be relatively small when compared to changes driven by precipitation and evaporation.

To calculate the predicted $\delta^{18}O$ value of calcite precipitating in Qilu today, we used Equation (1) where T = 20 °C (the mean June, July, August temperature of Kunming) and the lake water $\delta^{18}O$ value = −4.25‰ VSMOW from May 2019. Calcite precipitating in isotopic equilibrium with the lake water should therefore have a $\delta^{18}O$ value of −6.49‰ VPDB. The isotopic composition of the most recent surface sediments is −5.76‰ VPDB, in reasonable agreement with theoretical estimations and only +0.73‰ higher than expected. There are several possible reasons for this slight offset. First, there is some degree of uncertainty in the timing of calcite precipitation and while it most likely occurs in the summer when primary productivity is highest and results in the most rapid drawdown of CO_2, we have not personally observed this nor have any measurements to verify this. Second, small differences may occur between the June, July, August air temperature and lake water temperature. Nevertheless, given the relatively close agreement between theoretical and actual calcite values, we surmise that most calcite precipitating within the water column today is doing so in equilibrium.

The high covariance for the majority of the Qilu record (6.2−1.5 ka) ($R^2 = 0.85$, $p < 0.01$) (Fig. 5) also supports our assertion that Qilu behaves as a closed-basin lake and has remained as such throughout most of the Holocene (Horton et al., 2016). Typically lakes that have covariance with an $R^2 > 0.70$ are interpreted to be closed-basin and indicative of lake hydrological balance through time (Talbot, 1990). However, it should be noted that the lack of a strong R^2 covariance does not preclude a lake from being closed as there could be other complicating factors such as high alkalinity or lake level stabilization (Li and Ku, 1997). Therefore the lower covariance in Qilu isotopes from 1.5 ka to present ($R^2 = 0.30$, $p < 0.01$) does not necessarily suggest that Qilu instead behaved as an open−basin lake. Reasons and mechanisms that might explain this switch to lower covariance are considered in detail in section 5.5.

In the modern-day GNIP station data, the lowest $\delta^{18}O$ values in Kunming precipitation occur during the months of July and August when the ISM is at its peak. Traditionally, paleo-monsoon oxygen isotope records interpret lower $\delta^{18}O$ values to reflect a more intense period of monsoon activity (Wang et al., 2005). While this does not necessarily imply more monsoonal rainfall at a particular site, it reflects more intense monsoonal convection and upstream rainout (Vuille et al., 2005; Zhou et al., 2019). We therefore interpret lower $\delta^{18}O$ values in this context to reflect increased ISM strength and/or reduced evaporation. Higher $\delta^{18}O$ values are interpreted as being indicative of either reduced ISM strength and/or increased evaporation, driving isotopic enrichment of the lake water. As with any closed-basin lake, when there are substantial variations in lake level, the surface area to volume ratio may change along the lake bathymetric profile as well as nearshore catchment areas; if surface area/volume ratio increases substantially, this can increase evaporation rates, and vice versa (Steinman and Abbott, 2013).

In order to compare our results to the previous study by Hodell et al (1999), we plotted carbonate content and $\delta^{18}O$ values by both depth and age (Figs. S2 and 3). When compared by depth, there are many similar features in both measurements, although our study has a longer sequence of gradually increasing carbonate content and higher $\delta^{18}O$ values from 3.0 to 1.5 m than the same sequence in Hodell et al (1999) that spans from 1.5 to 1.0 m. Although the core collection location in Hodell et al (1999) was closer to the shoreline in a slightly shallower depth, it was not situated close to any inflowing streams, so sedimentation rates should be fairly comparable to our own coring site. However, as previously mentioned, the role of tectonic delivery is uncertain and may account for some of these differences. Additionally, sediment focusing may play a role within the basin. Our core was taken from the deepest part of the lake whereas the Hodell et al (1999) core was from a shallower area; therefore, our coring location may experience more sediment focusing.

An additional notable difference is the upper 1 m of both records, which is the red, iron-rich clay unit as indicated by the precipitous decline in carbonate content. The Hodell et al (1999) study suggests this begins ~1.0 m, which is estimated to be 2100 cal years BP whereas our study suggests this began ~0.6 m, estimated to be 1100 cal years BP. There was no age control within the upper 1.0 m of Qilu sediment in Hodell et al (1999) study, which can likely account for these large differences in timing. Ages from 1.0 m to the top were extrapolated, which also leads to some of the Hodell et al (1999) data being plotted as many hundreds of years into the future. In our study, $\delta^{18}O$ values reach their peak at 50 cm and the Hodell et al (1999) study does not have this pronounced peak, perhaps because of lower sampling resolution and/or differences in evaporation rates due to bathymetric characteristics at each coring location.

5.2. Unit I (6.2−5.2 ka)

There is some degree of estimation in the age of the base of this unit since it extends beyond the last radiocarbon date, but Unit I certainly extends to some time prior to 5.2 ka. This unit encompasses the period of lowest $\delta^{18}O$ values, suggesting the strongest

ISM precipitation of the record presented here and/or the lowest evaporation rates. Both $\delta^{18}O$ and $\delta^{13}C$ values slightly increase through this unit by 0.7‰ and 0.2‰, respectively, which is likely due to evaporative effects and CO_2 loss through degassing. Many paleorecords throughout SE Asia have identified a stronger early to middle Holocene ISM that gradually declines into the later Holocene as northern hemisphere summer insolation decreases, albeit with a slight lag between peak insolation values and peak ISM strength (e.g., Bird et al., 2014; Cheng et al., 2012; Kudrass et al., 2001). One additional factor that may be important is the seasonality of precipitation. Since modern-day precipitation tends to have lower $\delta^{18}O$ values in the summer than the winter due to rain-out and distillation, a shift in the proportion of summer versus winter precipitation may also account for the relatively lower $\delta^{18}O$ values observed at Qilu in Unit I.

However, because this portion of the record does take place in a period closer to what the International Commission on Stratigraphy defines as the middle Holocene (8.3–4.2 ka) (Cohen et al., 2019) when summer insolation is gradually decreasing, while ISM strength is stronger than present-day, it is gradually weakening. Since Xingyun is another lake that behaves as a closed-basin and is ~10 km to the north of Qilu, they have a similar surface area, and it was also previously studied by Hodell et al (1999), we make direct comparisons between Xingyun and Qilu (Fig. 6). A previous high-resolution study of Xingyun found gradually increasing $\delta^{18}O$ values during this time period, which were interpreted to reflect a combination of gradually declining ISM strength as well as gradually increasing evaporation, driving $\delta^{18}O$ values higher (Hillman et al., 2017). There may be some combination of similar processes occurring at Qilu, but they are not fully captured because our record does not extend back far enough. The $\delta^{18}O$ values in Qilu are similar to the values in Xingyun, albeit with a fairly constant offset of ~1‰, which may be due hydrology differences, evaporation rates, or the difference in catchment area size (200 km^2 at Qilu versus 383 km^2 at Xingyun). Nonetheless, these similar values suggest that the lakes are responding to comparable processes across much of this time period or that the lakes may be hydrologically connected through groundwater throughflow in this karstic region.

5.3. Unit II (5.2–3.6 ka)

This unit is characterized by increasing $\delta^{18}O$ values, first rapidly by 1.12‰ over 600 years, and then more gradually by 1.00‰ over 1200 years. While the rapidity of these events may be attributable to changing sedimentation rates in the Qilu age model, these shifts are remarkably similar in timing, magnitude, and rate to major $\delta^{18}O$ shifts at Xingyun (Fig. 6). Previously this was interpreted at Xingyun to be primarily driven by evaporative processes which resulted in higher $\delta^{18}O$ values and ultimately caused lower lake levels (Hillman et al., 2017). Evaporation was considered to be the primary cause of this trend, rather than decreasing precipitation amounts, because a palynological mean annual precipitation reconstruction from Xingyun sediments only suggested a ~10% decline in precipitation over this period which cannot account for such large magnitude shifts (Chen et al., 2014).

We interpret the $\delta^{18}O$ shift at Qilu to be similarly driven by increased evaporation rates because vegetation responses to precipitation are likely very similar across the 10 km distance between lake catchments, and changes in temperature must be unreasonably large to wholly account for the shift (+7.4 °C over 1800 years). It is possible that some degree of temperature change may be attributable to this large $\delta^{18}O$ shift as some other palynological based temperature reconstructions from Yunnan lakes do suggest slightly warming conditions through this period (Shen et al., 2006; Song et al., 2011; Xiao et al., 2014); however, these reconstructions do not suggest that such a large and rapid 7.4 °C increase in 1800 years is reasonable. Additionally, comparison of both Qilu and Xingyun records to Dongge Cave, 500 km to the east and traditionally interpreted as reflecting monsoon strength, shows that they diverge most rapidly at 5.2 ka and strongly suggests the influence in evaporative enrichment at the lakes (Wang et al., 2005) (Fig. 7).

Therefore, we interpret Unit II to reflect a drop in lake levels driven by increasing aridity. The increase in $\delta^{13}C$ values that occurs

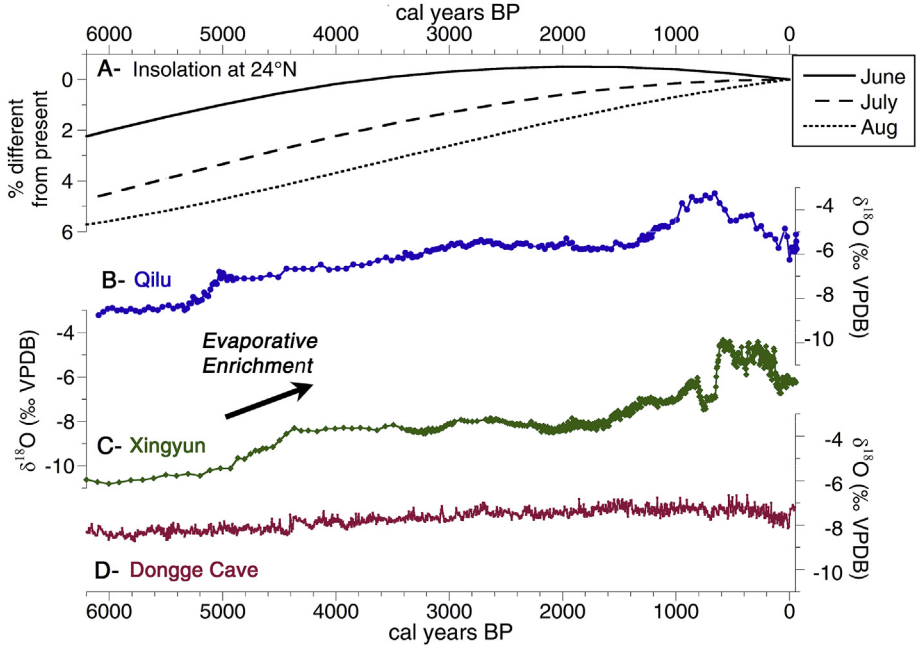

Fig. 6. A) June, July, August insolation at 24°N expressed as percent different from present-day; B) Qilu oxygen isotopes from this; C) Xingyun oxygen isotopes from Hillman et al. (2017); D) Dongge cave oxygen isotope from Wang et al. (2005). Note that all isotope records are on the same scale.

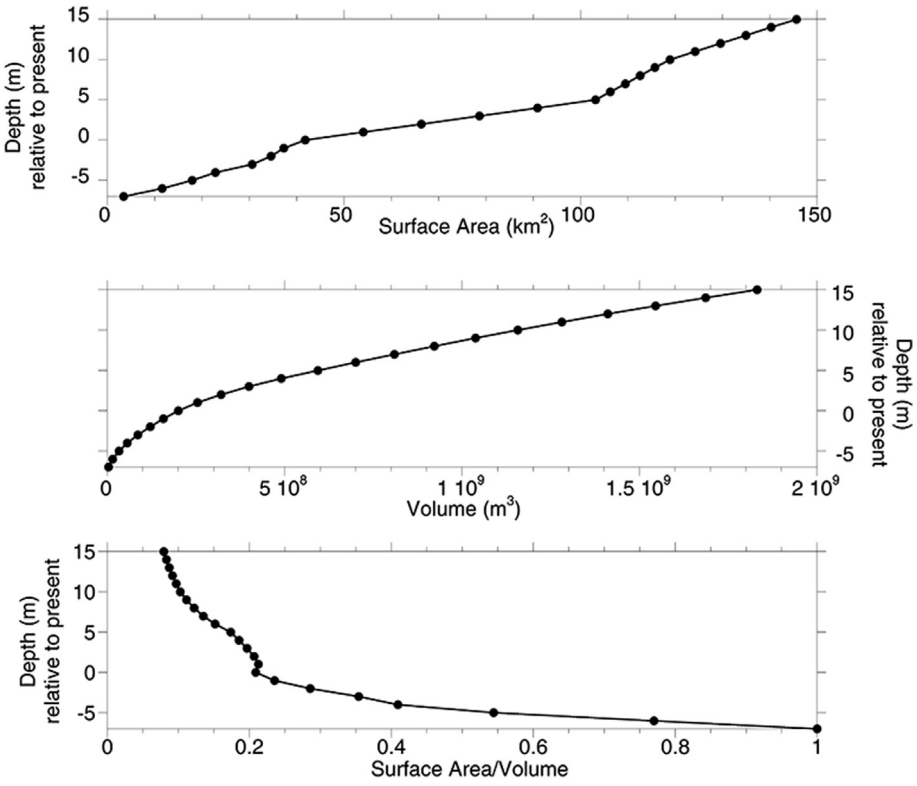

Fig. 7. A) Surface area profile; B) Volumetric profile; C) Surface area to volume ratio profile.

concomitantly with the initial increase in $\delta^{18}O$ values is likely due to the influence of lake level on CO_2 evasion (Fig. 4). As lake level decreases, CO_2 degassing as well as increased primary productivity stimulated by overturn, results in increased CO_2 evasion rates (Li and Ku, 1997), which drives $\delta^{13}C$ to higher values. $\delta^{13}C$ values in Qilu do not continue the uninterrupted gradual positive trend that is displayed in the $\delta^{18}O$ values, but this may be due to other factors such as the influence of variable primary productivity. Increasing amounts of carbonate material through this unit may also be attributable to declines in lake level as CO_2 reaches saturation and precipitates out as authigenic $CaCO_3$.

The fact that both Qilu and Xingyun display a rapid shift to higher $\delta^{18}O$ values followed by a more gradual trend suggests that a regional change in aridity is responsible. Abrupt shifts in hydroclimate during this period have been noted by several types of records in the ISM region. This arid interval is observed in cave records from south central Tibet (Cai et al., 2012) and northeast India (Berkelhammer et al., 2012), in lake and peat records from central India (Sarkar et al., 2015) and southwestern China (Hong et al., 2014), and in ocean cores from the Andaman Sea (Gebregiorgis et al., 2016) and Bay of Bengal (Govil and Naidu, 2011). The peak timing of this interval is slightly different in each record but they are all broadly centered on the period from 5 to 4 ka. Notably however, this feature is not extremely pronounced in monsoon records from further east such as Dongge Cave (Wang et al., 2005) and Sanbao Cave (Dong et al., 2010).

Several explanations for these shifts have been proposed. Fleitmann et al. (2007) hypothesize that the gradual decline of the ISM driven by declining summer insolation caused a southward shift of the ITCZ. However, other researchers make links to discrete events such as Bond event 3 (Hong et al., 2014) or the increased frequency of El Niño events causing shifts in the Walker circulation (Zhao et al., 2016) or a more positive IOD-like mean state (Abram et al., 2009). Unfortunately it is difficult to quantify the precipitation anomalies that might be driven by each process since El Niño and positive IOD events are inextricably linked, but the results from Qilu and Xingyun tend to support hypotheses that favor abrupt events rather than gradual changes, although this is dependent on accurate chronology.

A gradually weakening ISM might result in more evaporation due to fewer clouds in the sky and could account for some degree of gradual changes. However, successive El Niño events or a more positive IOD mean state causing abrupt arid periods would better explain the rapid nature of the $\delta^{18}O$ shifts. This is particularly true since the Qilu catchment does not display rapid changes in surface area to volume ratio at levels above present-day (Fig. 7). If surface area to volume ratio rapidly declined as lake levels dropped towards present-day, this might have created a "tipping point" in which gradual changes in P-E balance may have resulted in rapid changes in lake level. However, while surface area to volume ratios do increase from 15 to 0 m higher than present-day, they do not do so rapidly or at any particular threshold. This would suggest that the rapid increase in $\delta^{18}O$ values at Qilu is not driven by a nonlinear response arising from lake bathymetry but does represent an abrupt shift in P-E balance.

5.4. Unit III (3.6–1.5 ka)

Unit III is characterized by fairly stable $\delta^{18}O$ and $\delta^{13}C$ values. $\delta^{18}O$ values are slightly more variable than $\delta^{13}C$ values and increase over the entirety of the unit by 0.60‰, but in comparison to other units, do not show major fluctuations. Through this period, summer insolation particularly in July and August continued to decline (Fig. 6) which would result in a weak ISM, less upstream air mass convection and distillation, and higher $\delta^{18}O$ values in precipitation, coupled by continued increasing evaporation rates from reduced

cloud cover. However, despite these broad trends that would result in higher $\delta^{18}O$ values, isotopes at Qilu do not reflect this to a large degree.

Again, this is extremely similar to previous work at Xingyun, which also found stable $\delta^{18}O$ values from 3.0 to 1.5 ka (Hillman et al., 2017), although we note that this section of the Qilu core has the greatest age uncertainty associated with it, and therefore the synchronicity of events is subject to wide 95% confidence intervals. The stable values at Xingyun were interpreted to be a period of relative stability in lake level partly arising from a weak ISM. However, the $\delta^{18}O$ values at Xingyun were also partially attributed to a unique lake bathymetry where lake level fluctuations between 4 and 0 m higher than present-day do not result in changes in surface area to volume ratio and thereby limit evaporation rates and lake water isotopic enrichment. It is possible that similar processes are occurring at Qilu, however, as previously discussed, an analysis of surface area and volume profiles over 15 m higher than present-day and 7 m lower than present-day (lake bottom) does not reveal any similar bathymetric tipping points (Fig. 7). At Qilu, any lake level changes that result in fluctuations in volume also result in commensurate fluctuations in surface area and there are fewer constraints on the limits of evaporative enrichment. Therefore, Unit III likely represents a period of lake level stability at Qilu. This may also explain why $\delta^{13}C$ values are relatively invariant because stable lake levels facilitate CO_2 vapor exchange with the atmosphere which allows $\delta^{13}C$ values to reach equilibrium and remain steady (Li and Ku, 1997).

Since Xingyun and Qilu once again show remarkable agreement with a constant 1‰ offset, it may be that Xingyun $\delta^{18}O$ values are less controlled by lake bathymetric characteristics than previously thought, and instead are more reflective of a real period of lake level stability driven by regional climate stability. ENSO variability in the late Holocene is still debated with several records showing evidence for increasingly frequent El Niño events from 5.0 ka to present (Conroy et al., 2008; Koutavas et al., 2006; Moy et al., 2002), although not all records display this trend (Cobb et al., 2013). If El Niño events were increasing in frequency through this period and were a dominant control on centennial-scale variability, we would expect weaker ISM conditions, not persistently stable ones. Alternatively, the reconstructed IOD index is neither strongly positive nor negative (Abram et al., 2009), suggesting some degree of stability that may explain this period. However, additional records will be necessary to fully explore this stability and we cannot determine the ultimate forcing with our existing data.

5.5. Unit IV (1.5 ka-present)

Both $\delta^{18}O$ and $\delta^{13}C$ values display their greatest variability and most rapid change in Unit IV. Initially both $\delta^{18}O$ and $\delta^{13}C$ increase, suggesting that this may be driven by lower lake levels, causing isotopic enrichment of both elements due to increased evaporation and CO_2 evasion rates. However, shortly thereafter at 1.2 ka, $\delta^{18}O$ and $\delta^{13}C$ values rapidly diverge as $\delta^{18}O$ continues to increase and $\delta^{13}C$ declines, leading to lower covariance through this unit (Fig. 5). This divergence is closely followed by increasing magnetic susceptibility values at 1.0 ka and then the appearance of the red, iron-rich clay layer and the decline in weight percent carbonate content at 0.6 ka (Fig. 4). Similar units have previously been observed in other nearby lakes such as Xingyun and Dian and have been interpreted to be the result of anthropogenic land clearance and catchment sediment erosion (Hillman et al., 2014, 2019).

The rapid and very large decline in $\delta^{13}C$ values will be explored in detail in a separate manuscript. This large magnitude change likely indicates profound changes in the lake's carbon cycling since a lake's dissolved inorganic carbon cycle can be tied to changes in primary productivity, terrestrial organic matter inputs, and release of CO_2 from the oxidation of organic materials (Leng and Marshall, 2004). A full exploration of these connections is beyond the principle focus of this manuscript on lake hydrologic balance. However, when taken together with the composition of the sediment, the isotopic shifts in Unit IV are indicative of substantial human activity within the lake catchment. Similar sedimentological units have been noted at nearby lakes Xingyun at 1.5 ka (Hillman et al., 2014) and Dian at 1.8 ka (Hillman et al., 2019) and have been interpreted to be the result of land use change, deforestation, and sediment inwash of catchment soils. Brenner et al. (1991) noted these sedimentological changes at Qilu as well and also ascribed them to human activities, but the timing in that study was more uncertain and thought to be more recent. With increasing amounts of soil washing into the lake, the carbon cycle was likely greatly perturbed and can account for the divergent trends in $\delta^{18}O$ and $\delta^{13}C$; therefore, the lower covariance through Unit IV (Fig. 5) does not necessarily imply that Qilu was no longer behaving as a closed-basin.

Known periods of hydroclimate change around this time include the Medieval Climate Anomaly (MCA) from 1050 to 850 cal years BP and the Little Ice Age (LIA) from 650 to 150 cal years BP. While both periods can have indistinct temporal and spatial boundaries, previous work in SE Asia has found evidence for a stronger ISM during the MCA and a weaker ISM during the LIA (Bird et al., 2016; Hong et al., 2003; Morrill et al., 2003). Neither of these periods then can explain the initial lake level drop at 1500 cal years BP at Qilu nor does a stronger ISM during the MCA coincide with the inferred lake level increase after 750 cal years BP. Therefore it is highly likely that the shifts are driven by human manipulations of hydrologic balance.

Terraced rice agriculture was introduced in the Yunnan region around 2.2 ka (Herman, 2002), although this terracing was initially limited to upland areas which may explain why measurable anthropogenic impacts to lake level do not appear until several hundreds of years later. The initially gradual and then more rapid increase in $\delta^{18}O$ values are likely a result of the intensification of agriculture and the withdrawal or capture of inflowing water. Qilu bathymetric profiles indicate that as lake levels drop below present-day, surface area to volume ratio rapidly increases, even over a depth change of only a few meters (Fig. 7). A rapid increase in surface area to volume ratio would increase evaporation rates and lead to further isotopic enrichment. This may explain why $\delta^{18}O$ values first gradually get higher before rapidly reaching a peak. Similarly, initial increases in $\delta^{13}C$ values in Unit IV up to +7.39‰ may be driven by this evaporative loss and CO_2 degassing. The large and rapid shift to lower values that follows requires further investigations, but possible mechanisms include the oxidation of organic matter or the influx of soil organic carbon (Leng and Marshall, 2004).

Additionally, there is evidence of extensive anthropogenic land-building on the southern and western shores of Qilu. Although it is unknown when this land-building took place, it would have served as an additional driver of decreased lake volume, further increasing surface area to volume ratio. The timing of these initial changes in lake level at Qilu at 1.5 ka are synchronous with initial shifts in Xingyun $\delta^{18}O$, interpreted to be driven by similar anthropogenic processes. This may indicate similar human activities within each catchment driven by their proximity and the possible migration and diffusion of hydrologic modification technology.

$\delta^{18}O$ values shift back to lower values indicative of higher lake levels around 750 cal years BP. A similar period of high lake levels occurred at Xingyun from 680 to 570 cal years BP and was interpreted to be the result of the construction of a dam on an outflowing river (Hillman et al., 2014). However, $\delta^{18}O$ values at

Xingyun rapidly returned to higher values after a 110 year period, which was coincident with multiple occurrences of trenching of the outflowing river (Fig. 6). This was also concurrent with the intensification of rice agriculture driven by expanding populations within the greater Kunming region (Durand, 1960; Herman, 2002). Qilu isotopes on the other hand continue a declining trend towards present-day and do not exhibit further increases in $\delta^{18}O$ values which would be indicative of lake level declines. This is additionally surprising because a weaker ISM during the LIA would have acted to further drive lake levels lower. This warrants further investigation, but may suggest that human manipulation aimed at intentionally created higher than normal lake levels was taking place at Qilu after 750 cal years BP; however, there are no historical records to verify this. The outflow channel that would discharge lake water into the karst system is presently blocked off to facilitate irrigation, but it is unknown when this modification took place. The initiation of this modification after 750 cal years BP may account for this trend towards higher lake levels.

6. Conclusion

The 6200 year sediment record from Qilu Lake documents the precessional-scale decreasing strength of the ISM over the middle to late Holocene, albeit with a slight lag between peak insolation values and peak ISM strength, as well multicentennial-scale variability in hydrologic balance. Further, after 1500 BP there is an increasingly intense anthropogenic imprint on lake hydrologic balance from human development and erosion. One of the most striking features of the record is a large magnitude shift in $\delta^{18}O$ values from 5200 to 3600 cal years BP that can be largely attributed to higher evaporation rates rather than decreased precipitation amounts or increased temperatures; this is especially apparent when compared to speleothem records of monsoon strength such as Dongge Cave. These changes are remarkably similar in timing and magnitude to isotope shifts observed at nearby Xingyun Lake, supporting the idea that this is a regional climate signal. Records throughout the ISM region note this period of aridity as well, suggesting that although Yunnan lies within the ISM and EASM transition zone, the ISM likely plays a more important role. From 3600 to 1500 cal years BP, both Qilu and Xingyun lake levels are remarkably stable, which may suggest a period of regional climate stability, the cause of which requires further investigation.

After 1500 cal years BP, $\delta^{18}O$ values at Qilu are more impacted by anthropogenic forcings rather than climatic ones. The intensification of rice agriculture within the region likely resulted in increased water demand causing diversion and withdrawal that led to higher rates of evaporation and lower lake levels. However, differing water resource use led to different lake level trends between Qilu and Xingyun. The last 750 years of the Qilu isotope record diverges substantially from Xingyun and suggests a return to higher lake levels. This may have been driven by anthropogenic modification of the lake outflow in order to maintain a constant source of water for irrigation. The Qilu record of the last 1500 years suggests a complex interplay between ISM strength and the need for freshwater resources in a rapidly expanding population.

Data availability

Datasets related to this article can be found at https://data.mendeley.com/datasets/yg3x2pfdkn/1, an open-source online data repository hosted at Mendeley Data.

Declaration of competing interest

None.

Acknowledgments

This project was supported by an NSF-EAR Geomorphology and Land Use Dynamics grant to Aubrey Hillman (#1648634) and Daniel Bain and Mark Abbott (#1648772). We thank David Dettman for the analysis of stable isotopes and Duo Wu for assistance with fieldwork. We thanks two anonymous reviewers for their helpful comments and feedback which greatly improved the quality of this manuscript.

Appendix A. Supplementary data

Supplementary data to this article can be found online at https://doi.org/10.1016/j.quascirev.2019.106051.

References

Abbott, M.B., Stafford, T.W., 1996. Radiocarbon geochemistry of modern and ancient arctic lake systems, Baffin Island, Canada. Quat. Res. 45, 300–311.
Abram, N.J., Gagan, M.K., Cole, J.E., Hantoro, W.S., Mudelsee, M., 2008. Recent intensification of tropical climate variability in the Indian Ocean. Nat. Geosci. 1, 849–853.
Abram, N.J., Gagan, M.K., Liu, Z., Hantoro, W.S., McCulloch, M.T., Suwargadi, B.W., 2007. Seasonal characteristics of the Indian Ocean Dipole during the Holocene epoch. Nature 445, 299–302.
Abram, N.J., McGregor, H.V., Gagan, M.K., Hantoro, W.S., Suwargadi, B.W., 2009. Oscillations in the southern extent of the Indo-Pacific warm Pool during the mid-Holocene. Quat. Sci. Rev. 28, 2794–2803.
Araguás-Araguás, L., Froehlich, K., Rozanski, K., 1998. Stable isotope composition of precipitation over southeast Asia. J. Geophys. Res. 103, 721–742.
Berkelhammer, M., Sinha, A., Stott, L.D., Cheng, H., Pausata, F.S.R., Yoshimura, K., 2012. An Abrupt Shift in the Indian Monsoon 4000 Years Ago. American Geophysical Union.
Berry, G., Reeder, M.J., 2014. Objective identification of the intertropical convergence zone: climatology and trends from the ERA-interim. J. Clim. 27, 1894–1909.
Binford, M.W., 1990. Calculation and uncertainty analysis of ^{210}Pb dates for PIRLA project lake sediment cores. J. Paleolimnol. 3, 253–267.
Bird, B.W., Lei, Y., Perello, M., Polissar, P.J., Yao, T., Finney, B., Bain, D., Pompeani, D., Thompson, L.G., 2016. Late-Holocene Indian summer monsoon variability revealed from a 3300-year-long lake sediment record from Nir'pa Co, southeastern Tibet. Holocene 27, 541–552.
Bird, B.W., Polisar, P.J., Lei, Y., Thompson, L.G., Yao, T., Finney, B.P., Bain, D.J., Pompeani, D.P., Steinman, B.A., 2014. A Tibetan lake sediment record of Holocene Indian summer monsoon variability. Earth Planet. Sci. Lett. 399, 92–102.
Blaauw, M., Christen, J.A., 2011. Flexible paleoclimate age-depth models using an autoregressive gamma process. Bayesian Anal. 6, 457–474.
Brenner, M., Dorsey, K., Xueliang, S., Zuguan, W., Ruihua, L., Binford, M.W., Whitmore, T.J., Moore, A.M., 1991. Paleolimnology of Qilu Hu, Yunnan province, China. Hydrobiologia 214, 333–340.
Cai, Y., Zhang, H., Cheng, H., An, Z., Lawrence Edwards, R., Wang, X., Tan, L., Liang, F., Wang, J., Kelly, M., 2012. The Holocene Indian monsoon variability over the southern Tibetan Plateau and its teleconnections. Earth Planet. Sci. Lett. 335–336, 135–144.
Chen, F., Chen, X., Chen, J., Zhou, A., Wu, D.U.O., Tang, L., Zhang, X., Huang, X., Yu, J., 2014. Holocene vegetation history, precipitation changes and Indian Summer Monsoon evolution documented from sediments of Xingyun Lake, south-west China. J. Quat. Sci. 29, 661–674.
Cheng, H., Sinha, A., Wang, X., Cruz, F.W., Edwards, R.L., 2012. The global Paleomonsoon as seen through speleothem records from Asia and the Americas. Clim. Dyn. 39, 1045–1062.
Cobb, K.M., Westphal, N., Sayani, H.R., Watson, J.T., Di Lorenzo, E., Cheng, H., Edwards, R.L., Charles, C.D., 2013. Highly variable El Niño–southern oscillation throughout the Holocene. Science 339.
Cohen, K.M., Harper, D.A.T., Gibbard, P.L., 2019. ICS International Chronostratigraphic Chart 2019/05. International Commission on Stratigraphy. IUGS. www.stratigraphy.org.
Conroy, J.L., Overpeck, J.T., Cole, J.E., Shanahan, T.M., Steinitz-Kannan, M., 2008. Holocene changes in eastern tropical Pacific climate inferred from a Galápagos lake sediment record. Quat. Sci. Rev. 27, 1166–1180.
Craig, H., 1965. The measurement of oxygen isotope palaeotemperatures. In: Tongiorgi, E. (Ed.), Stable Isotopes in Oceanographic Studies and Palaeotemperatures. Consiglio Nazionale delle Ricerche Laboratorio di Geologia Nucleare, Pisa.
Dean, W.E., 1974. Determination of carbonate and organic matter in calcareous sediments and sedimentary rocks by loss on ignition: comparison with other methods. J. Sediment. Petrol. 44, 242–248.
Deevey, E.S., Gross, M.S., Hutchinson, G., Kraybill, H.L., 1954. The natural C14 contents of materials from hard-water lakes. Geology 40, 285–288.
Dong, J., Wang, Y., Edwards, R.L., Chen, S., Liu, D., Cheng, H., Kong, X., Jiang, X.,

Hardt, B., Wu, J., Zhao, K., 2010. A high-resolution stalagmite record of the Holocene East Asian monsoon from Mt Shennongjia, central China. Holocene 20, 257–264.
Durand, J.D., 1960. The population statistics of China, A.D. 2-1953. Popul. Stud. 13, 209–256.
Fleitmann, D., Burns, S.J., Mangini, A., Mudelsee, M., Kramers, J., Villa, I., Neff, U., Al-Subbary, A.A., Buettner, A., Hippler, D., Matter, A., 2007. Holocene ITCZ and Indian monsoon dynamics recorded in stalagmites from Oman and Yemen (Socotra). Quat. Sci. Rev. 26, 170–188.
Gebregiorgis, D., Hathorne, E.C., Sijinkumar, A.V., Nath, B.N., Nürnberg, D., Frank, M., 2016. South Asian summer monsoon variability during the last ~54 kyrs inferred from surface water salinity and river runoff proxies. Quat. Sci. Rev. 138, 6–15.
Geyh, M.A., Schotterer, U., Grosjean, M., 1997. Temporal changes of the 14C reservoir effect in lakes. Radiocarbon 40 (2), 921–931.
Govil, P., Naidu, P.D., 2011. Variations of Indian monsoon precipitation during the last 32kyr reflected in the surface hydrography of the Western Bay of Bengal. Quat. Sci. Rev. 30, 3871–3879.
Herman, J., 2002. The mongol conquest of dali: the failed second front. In: Cosmo, N.D. (Ed.), Warfare in Inner Asian History (500-1800). Brill, Boston.
Hillman, A.L., Abbott, M.B., Finkenbinder, M.S., Yu, J., 2017. An 8,600 year lacustrine record of summer monsoon variability from Yunnan, China. Quat. Sci. Rev. 174, 120–132.
Hillman, A.L., Yao, A., Abbott, M.B., Bain, D.J., 2019. Two millennia of anthropogenic landscape modification and nutrient loading at dian lake, Yunnan province, China. Holocene 29 (3), 505–517.
Hillman, A.L., Yu, J., Abbott, M.B., Cooke, C.A., Bain, D.J., Steinman, B.A., 2014. Rapid environmental change during dynastic transitions in Yunnan Province, China. Quat. Sci. Rev. 98, 24–32.
Hong, B., Hong, Y., Uchida, M., Shibata, Y., Cai, C., Peng, H., Zhu, Y., Wang, Y., Yuan, L., 2014. Abrupt variations of Indian and East Asian summer monsoons during the last deglacial stadial and interstadial. Quat. Sci. Rev. 97, 58–70.
Hong, B., Uchida, M., Hong, Y., Peng, H., Kondo, M., Ding, H., 2018. The respective characteristics of millennial-scale changes of the India summer monsoon in the Holocene and the Last Glacial. Palaeogeogr. Palaeoclimatol. Palaeoecol. 496, 155–165.
Hodell, D.A., Brenner, M., Kanfoush, S.L., Curtis, J.H., Stoner, J.S., Xueliang, S., Yuan, W., Whitmore, T.J., 1999. Paleoclimate of Southwestern China for the past 50,000 yr Inferred from Lake sediment records. Quat. Res. 52, 369–380.
Hong, Y.T., Hong, B., Lin, Q.H., Zhu, Y.X., Shibata, Y., Hirota, M., Uchida, M., Leng, X.T., Jiang, H.B., Xu, H., Wang, H., Yi, L., 2003. Correlation between Indian ocean summer monsoon and north Atlantic climate during the Holocene. Earth Planet. Sci. Lett. 211, 371–380.
Horton, T.W., Defliese, W.F., Tripati, A.K., Oze, C., 2016. Evaporation induced ^{18}O and ^{13}C enrichment in lake systems: a global perspective on hydrologic balance effects. Quat. Sci. Rev. 131, 365–379.
Kathayat, G., Cheng, H., Sinha, A., Berkelhammer, M., Zhang, H., Duan, P., Li, H., Li, X., Ning, Y., Edwards, R.L., 2018. Evaluating the timing and structure of the 4.2 ka event in the Indian summer monsoon domain from an annually resolved speleothem record from Northeast India. Clim. Past 14, 1869–1879.
Kottek, M., Grieser, J., Beck, C., Rudolf, B., Rubel, F., 2006. World Map of the Köppen-Geiger climate classification updated. Meteorol. Z. 15, 259–263.
Koutavas, A., deMenocal, P.B., Olive, G.C., Lynch-Stieglitz, J., 2006. Mid-Holocene El Niño–Southern Oscillation (ENSO) attenuation revealed by individual foraminifera in eastern tropical Pacific sediments. Geology 34, 993.
Kudrass, H.R., Hofmann, A., Doose, H., Emeis, K., Erlenkeuser, H., 2001. Modulation and amplification of climatic changes in the Northern Hemisphere by the Indian summer monsoon during the past 80 k.y. Geology 29, 63–66.
Kutzbach, J., 1981. Monsoon climate of the early Holocene: climate experiment with the earth's orbital parameters for 9000 Years ago. Science 214, 59–61.
Leng, M.J., Marshall, J.D., 2004. Palaeoclimate interpretation of stable isotope data from lake sediment archives. Quat. Sci. Rev. 23, 811–831.
Li, H.-C., Ku, T.-L., 1997. $\delta^{13}C$-$\delta^{18}O$ covariance as a paleohydrological indicator for closed-basin lakes. Palaeogeogr. Palaeoclimatol. Palaeoecol. 133, 69–80.
Liu, W., Li, S., Bu, H., Zhang, Q., Liu, G., 2012. Eutrophication in the Yunnan Plateau lakes: the influence of lake morphology, watershed land use, and socioeconomic factors. Environ. Sci. Pollut. Res. Int. 19, 858–870.
Liu, Y., Guo, H.C., Yu, Y.J., Huang, K., Wang, Z., 2007. Sediment chemistry and the variation of three altiplano lakes to recent anthropogenic impacts in southwestern China. Water S.A. 33, 305-301.
Morrill, C., Overpeck, J.T., Cole, J.E., 2003. A synthesis of abrupt changes in the Asian summer monsoon since the last deglaciation. Holocene 13, 465–476.
Moy, C.M., Seltzer, G.O., Rodbell, D.T., Anderson, D.M., 2002. Variability of El Nino southern oscillation activity at millennial timescales during the Holocene epoch. Nature 402, 162–165.
Olsson, I., 1986. Radiometric methods. In: Berglund, B. (Ed.), Handbook of Holocene Palaeoecology and Palaeohydrology. John Wiley and Sons, Chichester, pp. 273–312.
Prodhomme, C., Terray, P., Masson, S., Boschat, G., Izumo, T., 2014. Oceanic factors controlling the Indian summer monsoon onset in a coupled model. Clim. Dyn. 44, 977–1002.
R Core Development Team, 2008. R: A Language and Environment for Statistical Computing.
Rashid, H., England, E., Thompson, L., Polyak, L., 2011. Late glacial to Holocene Indian summer monsoon variability based upon sediment records taken from the Bay of Bengal. Terr. Atmos. Ocean. Sci. 22, 215–228.
Reimer, P.J., Bard, E., Bayliss, A., Beck, J.W., Blackwell, P.G., Ramsey, C.B., Buck, C.E., Cheng, H., Edwards, R.L., Friedrich, M., Grootes, P.M., Guilderson, T.P., Haflidason, H., Hajdas, I., Hatté, C., Heaton, T.J., Hoffmann, D.L., Hogg, A.G., Hughen, K.A., Kaiser, K.F., Kromer, B., Manning, S.W., Niu, M., Reimer, R.W., Richards, D.A., Scott, E.M., Southon, J.R., Staff, R.A., Turney, C.S.M., Plicht, J.v.d., 2013. INTCAL13 and marine 13 radiocarbon age calibration curves 0–50,000 years CAL BP. Radiocarbon 55, 1869–1887.
Rozanski, K., Araguás-Araguás, L., Gonfiantini, R., 1993. Isotopic patterns in modern global precipitation. In: Swart, P.K., Lohmann, K.C., Mckenzie, J., Savin, S. (Eds.), Climate Change in Continental Isotopic Records. American Geophysical Union, Washington, D.C.
Saji, N.H., Goswami, B.N., Vinayachandran, P.N., Yamagata, T., 1999. A dipole in the tropical Indian Ocean. Nature 401, 360–363.
Sarkar, S., Prasad, S., Wilkes, H., Riedel, N., Stebich, M., Basavaiah, N., Sachse, D., 2015. Monsoon source shifts during the drying mid-Holocene: biomarker isotope based evidence from the core 'monsoon zone' (CMZ) of India. Quat. Sci. Rev. 123, 144–157.
Shen, J., Jones, R.T., Yang, W., Dearing, J.A., Wang, S., 2006. The Holocene vegetation history of Lake Erhai, Yunnan province southwestern China: the role of climate and human forcings. Holocene 16, 265–276.
Song, X.-Y., Yao, Y.-F., Wortley, A.H., Paudayal, K.N., Yang, S.-H., Li, C.-S., Blackmore, S., 2011. Holocene vegetation and climate history at Haligu on the jade dragon snow mountain, Yunnan, SW China. Clim. Change 113, 841–866.
Steinman, B.A., Abbott, M.B., 2013. Isotopic and hydrologic responses of small, closed lakes to climate variability: hydroclimate reconstructions from lake sediment oxygen isotope records and mass balance models. Geochem. Cosmochim. Acta 105, 342–359.
Talbot, M.R., 1990. A review of the palaeohydrological interpretation of carbon and oxygen isotopic ratios in primary lacustrine carbonates. Chem. Geol. 80, 261–279.
Vuille, M., Werner, M., Bradley, R.S., Keimig, F., 2005. Stable isotopes in precipitation in the Asian monsoon region. J. Geophys. Res. 110.
Wang, E., Burchfiel, B.C., Royden, L.H., Liangzhong, C., Jishen, C., Wenxin, L., Zhiliang, C., 1998. Late Cenozoic Xianshuihe-Xiaojiang, Red River, and Dali Fault Systems of Southwestern Sichuan and Central Yunnan. Special Paper of the Geological Society of America, Geological Society of America, China.
Wang, Y., Cheng, H., Edwards, R.L., He, Y., Kong, X., An, Z., Wu, J., Kelly, M.J., Dykoski, C.A., Li, X., 2005. The Holocene Asian monsoon: links to solar changes and North Atlantic climate. Science 308, 854–857.
Wang, Y.J., Cheng, H., Edwards, R.L., An, Z.S., Wu, J.Y., Shen, C.C., Dorale, J.A., 2001. A high-resolution absolute-dated late Pleistocene Monsoon record from Hulu Cave, China. Science 294, 2345–2348.
Wen, X.-Z., Ma, S.-L., Xu, X.-W., He, Y.-N., 2008. Historical pattern and behavior of earthquake ruptures along the eastern boundary of the Sichuan-Yunnan faulted-block, southwestern China. Phys. Earth Planet. Inter. 168, 16–36.
Whitmore, T.J., Brenner, M., Jiang, Z., Curtis, J.H., Moore, A.M., Engstrom, D.R., Yu, W., 1997. Water quality and sediment geochemistry in lakes of Yunnan Province, southern China. Environ. Geol. 32, 45–55.
Wohlfarth, B., Skog, G., Possnert, G., Holmquist, B., 1998. Pitfalls in the AMS radiocarbon-dating of terrestrial macrofossils. J. Quat. Sci. 13 (2), 137–145.
Wright, H., Mann, D., Glaser, P., 1984. Piston corers for peat and lake sediments. Ecology 65, 657–659.
Xiao, X., Haberle, S.G., Shen, J., Yang, X., Han, Y., Zhang, E., Wang, S., 2014. Latest Pleistocene and Holocene vegetation and climate history inferred from an alpine lacustrine record, northwestern Yunnan Province, southwestern China. Quat. Sci. Rev. 86, 35–48.
Yunnan Province Bureau of Geology and Mineral Resources, 1990. Regional geology of Yunnan province. People's Republic of China, ministry of geology and mineral resources. Geol. Mem. Series 1, 21.
Zhang, K., 1988. The climate dividing line between SW and SE monsoons and their differences in climatology and ecology in Yunnan province of China. Climatol. Notes 38, 197–207.
Zhao, K., Wang, Y., Edwards, R.L., Cheng, H., Liu, D., Kong, X., Ning, Y., 2016. Contribution of ENSO variability to the East Asian summer monsoon in the late Holocene. Palaeogeogr. Palaeoclimatol. Palaeoecol. 449, 510–519.
Zhou, H., Zhang, X., Yao, T., Hua, M., Wang, X., Rao, Z., He, X., 2019. Variation of $\delta^{18}O$ in precipitation and its response to upstream atmospheric convection and rainout: a case study of Changsha station, south-central China. Sci. Total Environ. 659, 1199–1208.